Appl Phys A (2011) 105:233–238
DOI 10.1007/s00339-011-6495-9

Applied Physics A
Materials Science & Processing

Dispersion of laser droplets using H^+ ions and annealing effect on pulsed laser deposited nickel ferrite thin films

Rakesh Malik · S. Annapoorni · S. Lamba · S. Mahmood · R.S. Rawat

Received: 10 February 2011 / Accepted: 20 May 2011 / Published online: 19 July 2011

Abstract Nickel ferrite thin films were deposited by a pulsed laser deposition (PLD) technique on silicon substrate at room temperature in a vacuum of 5×10^{-5} mbar. The films were subjected to different annealing temperatures from 300–900°C and were also exposed to single shot energetic hydrogen ions using a Dense Plasma Focus (DPF) device. The changes induced in the films exposed at different distances from the top of the anode were investigated. The structural, morphological and magnetic properties of the annealed and exposed samples were investigated. X-ray diffraction (XRD) studies reveal the presence of a single phase of nickel ferrite after annealing. SEM micrographs indicate an increase in the grain size, both on annealing as well as on exposure to hydrogen ions. Annealing and hydrogen ion irradiation induced an enhancement in the magnetic moments. Laser droplets which are inherent in films deposited by laser ablation were found to be dispersed as a result of single shot hydrogen ion irradiation from the DPF.

R. Malik
Department of Physics, Atma Ram Sanatan Dharma College, University of Delhi, New Delhi, 110021, India

S. Annapoorni (✉)
Department of Physics and Astrophysics, University of Delhi, Delhi, 110 007, India
e-mail: annapoorni@physics.du.ac.in

S. Lamba
Indira Gandhi National Open University, Maidangarhi, Delhi, 110 068, India

S. Mahmood · R.S. Rawat
National Institute of Education, Nanyang Technological University, Singapore, Singapore

1 Introduction

Nickel ferrite is a soft ferrimagnetic material that crystallizes in an inverse spinal structure with Fe^{3+} ions distributed equally on tetrahedral and octahedral sites and Ni^{2+} ions on octahedral sites [1–3]. Spinel ferrites are widely used for applications like permanent magnets, recording media, ferrofluids, microwaves, sensors and as an anode material in lithium ion batteries [4–7]. Nickel ferrite thin films are usually prepared using chemical and physical methods like spin coating, spray pyrolysis, ferrite plating, sputtering, electrodeposition and pulsed laser deposition (PLD) [8–11]. The deposition of ferrite thin films by chemical methods has many drawbacks such as lack of uniformity and thickness control, improper stoichiometry and the possibility of the formation of other phases, thus limiting the use of thin films for practical applications. Sputtering techniques require a bigger-sized target. It is also difficult to maintain the high power for the longer time of deposition required to deposit films of sufficient thickness for characterization and application. Electrodeposition requires a conducting substrate to deposit the thin films, which limits its suitability in certain applications. In recent times, PLD techniques have emerged as an important method for depositing thin films of various materials. The PLD technique is a simple method, in which the target sizes required are fairly small and easy to prepare. Moreover, the films prepared by this method retain good stoichiometry, and the deposition rates are high [12]. The morphology and growth of the films can be controlled by varying the gas pressure, atmosphere, orientation and distance of the substrate from the target. However, the formation of laser droplets is an inherent problem of PLD deposited samples. Several in situ methods, viz., off-axis placement of substrate, using filters between target and substrate, spatial filters, van-type velocity filters, deposition under different gas

atmospheres, using double slit, and crossed magnetic fields, etc., have been employed to avoid the formation of laser droplets [13–15]. In many of these methods the reduction in the density of the droplets is accompanied by a poor deposition rate. In this report we present the results obtained on the thin films of nickel ferrite prepared using the PLD method. Nickel ferrite thin films thus prepared were subjected to different annealing temperatures and also exposed to energetic H^+ ions using a Dense Plasma Focus (DPF) device. The resulting changes in the structure and morphology of the thin films and the magnetic properties are reported in this paper. In Sect. 2 the experimental details for the preparation of the films are described, followed by the structural characterization and magnetic studies in Sect. 3. We present our conclusions in Sect. 4.

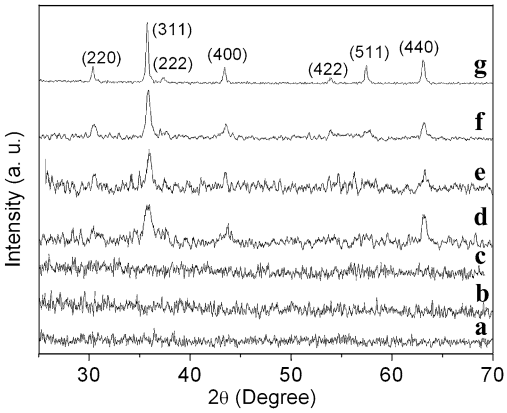

Fig. 1 XRD patterns for the nickel ferrite thin film sample (**a**) as-deposited, (**b**) irradiated at 5 cm and for the samples obtained after annealing the thin films at the temperatures of (**c**) 300, (**d**) 500, (**e**) 700, (**f**) 900°C and (**g**) nickel ferrite target used for deposition

2 Experimental details

Nickel ferrite particles of 98% purity (Aldrich Co.) were used to make the target. The target was sintered at 900°C for 10 h by the conventional sintering method before it was subjected to laser ablation. Thin films of nickel ferrite were deposited on a silicon substrate at room temperature by PLD. The ablation process of the nickel ferrite target was carried out in vacuum at a base pressure of $\sim 5 \times 10^{-5}$ mbar using the typical PLD setup. A continuum Surelite Nd:YAG laser (532 nm) laser beam with a pulse power of 30 mJ and repetition rate of 10 Hz was focused onto the $NiFe_2O_4$ target. The distance between the target and the substrate was maintained at 5 cm. Both the target and the substrate were rotated at a fixed rpm in order to obtain uniform films. The as-deposited $NiFe_2O_4$ thin films were annealed at different temperatures, viz., 300, 500, 700 and 900°C, for 3 h. The as-deposited $NiFe_2O_4$ thin films were also exposed to energetic H^+ ions using a single capacitor United Nation University/International Center for Theoretical Physics (UNU/ICTP) plasma focus device. A resistive divider with a 100 times attenuation was used as a voltage probe. The time span estimated for the energetic hydrogen ions is about a few hundred nanoseconds (ns). Using a Faraday cup, the energy of the hydrogen ions was found to vary in the range of 35–1500 keV with a mean energy of 124 keV per ion (Lin et al., [16]). It may, however, be mentioned that the energy of the ions on the lower energy side is actually lower than that reported in [16], as the typical threshold limit of ion energy measurement using a biased ion collector (Faraday cup) is typically around 25 keV [17] for deuterium ions and around 50 keV for nitrogen ions [18]. The energy of the ions may be as low as 10 keV for instability accelerated ions from the pinch region and even lower, a few hundred electron volts to a few kiloelectron volts, for the non-instability accelerated plasma in the radial phase. The nickel ferrite thin films were mounted horizontally on a vertically movable holder at an angle of 90° with respect to the direction of the energetic hydrogen ions [16].

The as-deposited thin film samples were exposed to H^+ ions using a single shot at different distances, viz., 5, 7 and 10 cm, from the top of the anode. The irradiations were performed at room temperature. The as-deposited sample, the annealed samples and those exposed to H^+ ion irradiation were subjected to different characterization studies and magnetic measurements. X-ray diffraction (XRD) data were collected in the glancing mode by using a SIEMENS D5000 diffractometer with Cu K$\alpha = 1.540$ Å radiation at 40 keV in the 2θ range from 25 to 70°. The film thickness was estimated to be 115–120 nm using X-ray reflectivity (XRR). The surface morphology and grain sizes were estimated by using a JEOL 6700F field emission scanning electron microscope (SEM). The M–H loop of the thin films was measured using a Quantum Design Magnetic Property Measurement System (MPMS) Superconducting Quantum Interference Device (SQUID) up to a field of 10 kOe at room temperature.

3 Results and discussion

3.1 X-ray diffraction

Figure 1 shows the XRD pattern of the nickel ferrite thin films and the thin films annealed at different temperatures along with that of the nickel ferrite target used for deposition. The XRD pattern of the as-deposited thin film and the film annealed at 300°C shows the amorphous nature, while the thin films annealed at 500, 700 and 900°C and the target used show the diffraction peaks of the nickel ferrite structure. The diffraction peaks are analyzed using Joint Committee on Powder Diffraction Standards (JCPDS) data [19],

and it is observed that the single-phase nickel ferrite structure has been retained for all the samples annealed at different temperatures [20]. It is observed that, as the annealing temperature increases from 500 to 900°C, the full width at half maximum decreases. This clearly indicates an evolution of the crystalline phase of the nickel ferrite structure when annealed above 500°C. The XRD analysis shows that the films exposed to single shot hydrogen ion irradiation remain amorphous in nature, indicating that the ion-induced transient thermal annealing is insufficient to induce any substantial crystallization, as shown in Fig. 1(b). A depth profile analysis of the hydrogen ions in the $NiFe_2O_4$ thin films was performed using the Stopping and Range of Ions in Matter (SRIM) 2003 software package [21]. The projected range of the hydrogen ions in the nickel ferrite films has been estimated to be 319 nm, 870 nm and 19 μm for 35 keV, 124 keV and 1500 keV energy of the hydrogen ions, respectively, which is much higher than the thickness of the thin film, ∼115 to 120 nm. This implies that the energetic hydrogen ions have enough energy to penetrate though and out of the nickel ferrite thin films; hence the changes induced by the energetic hydrogen ions can be considered to be uniform throughout the irradiated samples.

3.2 Scanning electron microscopy

The surface morphology of the nickel ferrite thin films has been studied using scanning electron microscopy (SEM). The SEM image for the as-deposited thin film and those annealed at 300 and 900°C along with the lognormal distribution of grain sizes are shown in Fig. 2. The grain sizes are estimated from a lognormal fit using the distribution data obtained from the SEM images. The average sizes are estimated to be 13, 17, 22 and 31 nm, respectively, for the as-deposited thin film and the thin films annealed at 500, 700 and 900°C. The SEM image of the as-deposited thin film (Fig. 2(a)) shows a homogeneous distribution of small grains all over the thin film surface, along with some bigger-sized grains. These bigger, random-sized grains of nickel ferrite over the surface of the thin films are generally referred to as laser droplets. The SEM image of the thin film annealed at 300°C shows a diffused pattern with no clear boundaries. With an increase in annealing temperature, an increase in the average grain size is observed. However, for annealing temperatures of 500°C and above, there is also a corresponding increase in the size of the laser droplets, as seen in the SEM image for the sample annealed at 900°C.

The SEM images for the samples irradiated by H^+ ions using a single DPF shot at a distance of 5, 7 and 10 cm from the top of the anode are shown in Figs. 3(a)–(c), respectively, along with the lognormal fit of the grain size distribution in the inset. The SEM image of the sample irradiated at 5 cm has an average grain size of 16 nm with the laser droplets

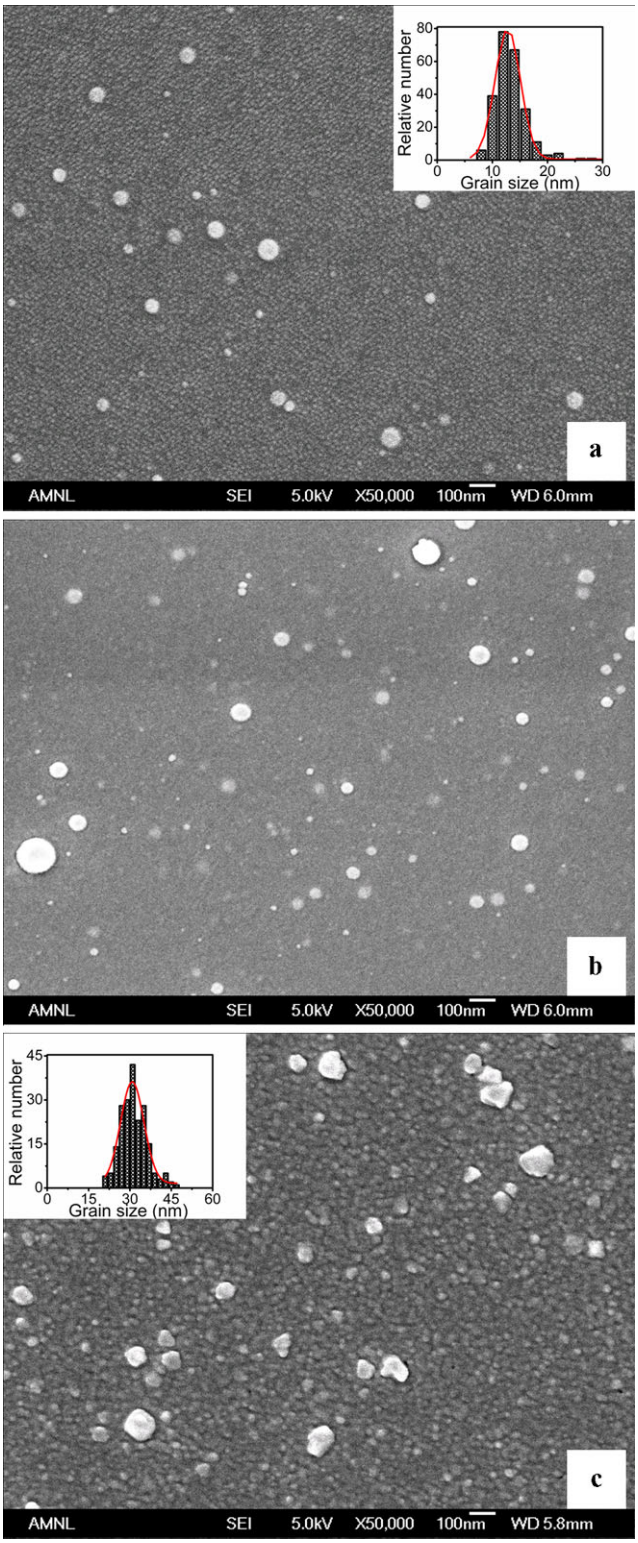

Fig. 2 SEM images of the nickel ferrite thin films (**a**) as-deposited sample and for the samples annealed at (**b**) 300 (**c**) 900°C. The grain size distribution appears as an *inset* in (**a**) and (**c**)

dispersed in the grain matrix, thereby showing a uniform morphology. On irradiation, a growth in the grain size is observed. The dispersion of the laser droplets in the matrix may be attributed to the interaction between the hydrogen ions, with a certain energy distribution, and the droplets [22, 23]. The energies of the hydrogen ions in a plasma focus device extend over a wide range. While the high energy ions will easily penetrate through the thickness of the $NiFe_2O_4$ film and deposit their energy essentially into the silicon substrate, the ions with a lower energy, a few hundred electron volts to a few kiloelectron volts (which also form the bulk of the ions) will not be able to penetrate through the films and will interact efficiently only with the surface layers of the films. This results in the breaking of the laser droplets on the surface and the grains present in the surface of the film. After the dispersion of the grains, the grains grow in size both due to the nuclear energy losses as well as the thermal energy deposited by the energetic ions in to the silicon substrate during the ion irradiation, which then conducts from the silicon substrate to the top surface layer. This was simultaneously confirmed from the SRIM calculations performed on the $NiFe_2O_4$ thin films for hydrogen ions with an average energy of 124 keV, which also confirmed both the presence of the nuclear energy loss and electronic energy loss. It is also understood that part of the energy deposited during the nuclear interaction results in grains boundary motion [24], which causes an increase in grain size. The remaining energy is thermalized in the lattice [25], which results in a temperature spike in small localized regions of the film and subsequent migration of atoms across the boundaries, leading to further grain growth [26].

From the SEM image of the sample irradiated at a distance of 7 cm (Fig. 3(b)) we find that there is no significant change in grain size (15 nm); however, there is a smaller number of laser droplets as compared to the as-deposited films. No dispersion of laser droplets was observed for the sample irradiated at 10 cm (Fig. 3(c)). Note that the thin film irradiated at a distance of 10 cm shows a similar surface morphology to the sample annealed at 300°C. The grain size in the sample irradiated at 7 cm is slightly more than that in the sample annealed at 300°C, but less than the grain size in the sample annealed at 500°C. It is reported that the energy of the ions and the fluence (ions/cm ^{2}) varies non-linearly with distance, specifically as the inverse square of the distance [27]. Thus the effect of irradiation over a larger distance is equivalent to subjecting the films to a lower annealing temperature. The change in energy and fluence of the energetic hydrogen ions results in a variation of grain sizes and surface morphology of the films. The irradiation with single shot H^+ ions leads to the breaking of laser droplets and introduces effects similar to annealing, depending on the distance of the exposure.

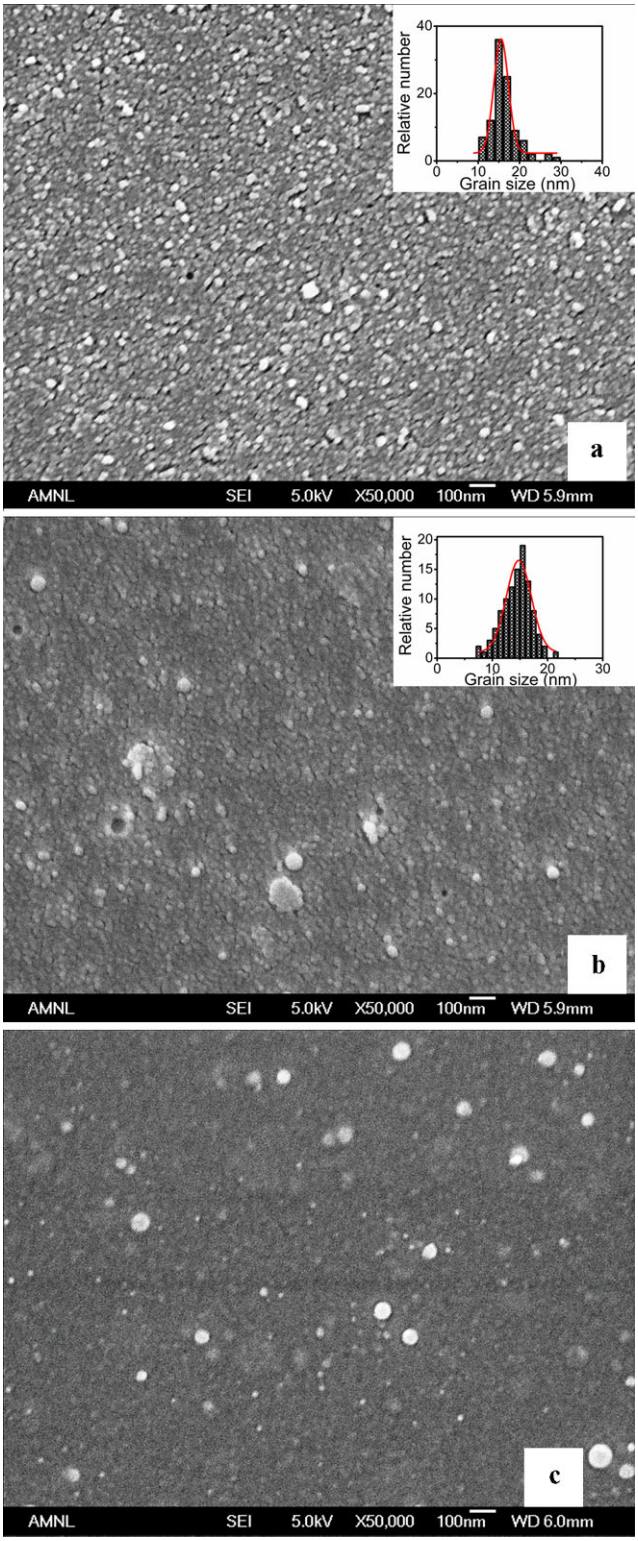

Fig. 3 SEM images of the nickel ferrite irradiated with single shot energetic H^+ ions at a distance of (**a**) 5, (**b**) 7 and (**c**) 10 cm from the anode. The grain size distribution appears as an *inset* in (**a**) and (**b**)

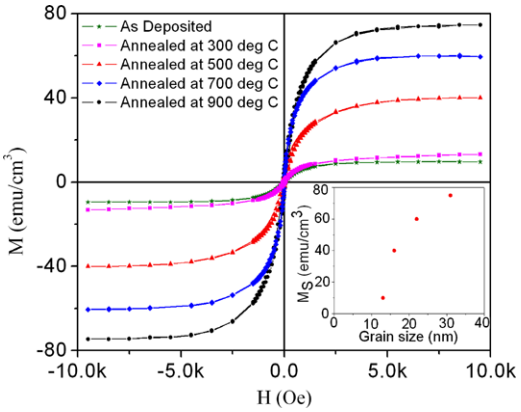

Fig. 4 Hysteresis measurement performed at 300 K for the as such deposited sample and samples annealed at 300, 500, 700 and 900°C temperatures

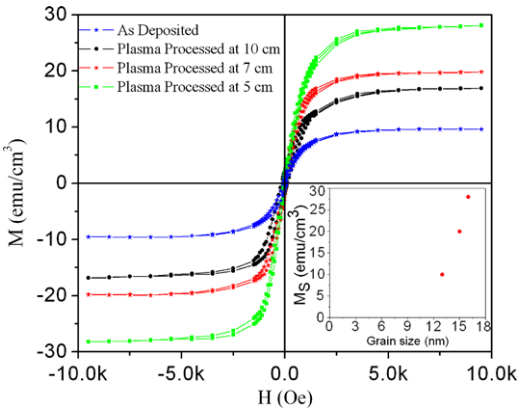

Fig. 5 Hysteresis measurement at 300 K for the samples irradiated with single shot energetic H^+ ions at a distance of 5, 7 and 10 cm

3.3 Magnetic measurements

The magnetic properties of the nickel ferrite thin films were investigated using a dc magnetometer. The hysteresis measurements were performed at room temperature for all the samples processed under different conditions. Figure 4 shows the hysteresis loop for the as such deposited thin film and the thin films annealed at 300, 500, 700 and 900°C. The hysteresis loop of the as-deposited thin film and the thin film annealed at 300°C does not show a tendency to saturate even up to a field of 10 kOe. This is due to the superparamagnetic behavior coupled with surface anisotropy. The samples annealed at 500, 700 and 900°C show a tendency towards saturation at the above mentioned field. This behavior of the hysteresis loop indicates a high surface anisotropy for the as-deposited samples and the samples annealed at lower temperatures. The inset in Fig. 4 shows the variation in the value of saturation magnetization with the grain size of the thin films annealed at different temperatures. The saturation magnetization is found to increase with increasing grain size [28]. The saturation magnetization is estimated by extrapolating the $1/H$ versus M curve. The maximum value of the saturation magnetization is observed to be 78 emu/cm^3 for the sample annealed at 900°C. A possible reason for the increase in saturation magnetization could be the decrease in the surface spin disorder with increasing grain size. The value of coercivity for the as- deposited sample and samples annealed at different temperatures is observed to be ∼78 Oe and 64 Oe, respectively. The change in the value of coercivity is not appreciable with the change in annealing temperature.

The response of the external applied magnetic field of the samples irradiated with energetic hydrogen ions at distances of 5, 7 and 10 cm from the top of the anode is given in Fig. 5. The hysteresis loops recorded for the irradiated thin films show a considerable change in the saturation magnetization and coercivity of the samples irradiated at different distances. The value of saturation magnetization is estimated to be 28, 20, 17 and 10 emu/cm^3 for the samples irradiated at 5, 7 and 10 cm and for the as-deposited sample, respectively. The value of saturation magnetization for the samples irradiated at 5, 7 and 10 cm distance is less than the value obtained for the sample annealed at 500°C (40 emu/cm^3), but higher than that of the samples annealed at 300°C (13 emu/cm^3). The inset in Fig. 5 shows the variation of saturation magnetization with the grain size for the samples irradiated at different distances. The value of saturation magnetization is found to increase with increasing grain size. The value of coercivity as determined from the hysteresis is found to be 78, 137, 64 and 54 Oe for the as-deposited sample and samples irradiated with hydrogen ions at 10, 7 and 5 cm respectively. The sample irradiated at 10 cm shows a maximum coercivity of about 137 Oe. The critical diameter of the nickel ferrite particles is ∼15 nm [29], and such an increase can be attributed to a change from single to multi-domain.

4 Conclusion

Nickel ferrite thin films of thickness 115 to 120 nm were prepared using PLD and are subjected to different annealing temperatures as well as exposed to energetic hydrogen ions using a DPF device. A single-phase nickel ferrite structure was observed in the PLD thin films after annealing. The presence of laser droplets, which are inherent in PLD films, was observed by SEM. A single shot irradiation of energetic hydrogen ions from a DPF device was found to dissolve the laser droplets, which is not achievable by annealing. The effect of the grain growth induced by ion irradiation is similar to the effect induced by thermal annealing on the surface morphology of the nickel ferrite thin films. An enhancement in magnetic properties of the thin films was observed both after annealing and after exposing the thin films to the energetic hydrogen ions. The hysteresis measurement shows

the change in the coercivity of the thin films irradiated at different distances by the hydrogen ions. To understand the changes induced in the magnetic properties of the thin films by the focused hydrogen ion, further investigation such as AC susceptibility and zero-field-cooled (ZFC)/field-cooled (FC) measurements should be performed.

Acknowledgements One of the authors (RM) wishes to acknowledge the University Grants Commission, India, for financial support and the National Institute of Education, Nanyang Technological University, Singapore, for extending their lab facilities for conducting a part of the research. The authors wish to acknowledge Professor Ratna Mala Chatterjee, Indian Institute of Technology, Delhi, India, for her help in carrying out the magnetic measurements.

References

1. W. Healy Daniel Jr., R.A. Johnson, Phys. Rev. **104**, 634 (1956)
2. L.G. Antoshina, A.B. Korshak, Phys. Solid State **51**, 949 (2009)
3. V.P.M. Shafi-Kurikka, Y. Koltypin, A. Gedanken, R. Prozorov, J. Balogh, J. Lendvai, I. Felner, J. Phys. Chem. B **101**, 6409 (1997)
4. B. Martinez, T. Obradors, L. Balcells, A. Rounanet, C. Monty, Phys. Rev. Lett. **80**, 181 (1998)
5. J. Ding, T. Reynolds, W.F. Miao, P.G. McCormick, R. Street, Appl. Phys. Lett. **65**, 3135 (1994)
6. C. Xiangfeng, J. Dongle, Z. Chenmou, Sens. Actuators A, Phys. **123**, 793 (2007)
7. R.H. Kodama, A.E. Berkowitz, E.J. McNiff, S. Foner, Phys. Rev. Lett. **77**, 394 (1996)
8. Y. Chung, S. Park, D. Kang, Mater. Chem. Phys. **86**, 375 (2004)
9. S. Venzke, R.B. Vandover, J.M. Phillips, E.M. Gyorgy, T. Siegrist, C.H. Chen, D. Werder, R.M. Fleming, R.J. Felder, E. Coleman, R. Opila, J. Mater. Res. **11**, 1187 (1996)
10. T. Tsuchiya, H. Yamashiro, T. Sci, T. Inamura, J. Mater. Sci. **27**, 3645 (1992)
11. B. Negulescu, L. Thomas, Y. Dumont, M. Tessier, N. Keller, M. Guyot, J. Magn. Magn. Mater. **242**, 529 (2002)
12. H. Kawasaki, K. Doi, S. Hiraishi, Y. Suda, Thin Solid Films **374**, 278 (2000)
13. T. Yoshitake, K. Nagayama, Vacuum **74**, 515 (2004)
14. K. Ebihara, S.M. Park, K. Fujii, T. Ikegami, Diam. Relat. Mater. **15**, 989 (2006)
15. T. Hino, S. Mustofa, M. Nishida, T. Araki, Vacuum **70**, 47 (2003)
16. J.J. Lin, M.V. Roshan, Z.Y. Pan, R. Verma, P. Lee, S.V. Springham, T.L. Tan, R.S. Rawat, J. Phys. D, Appl. Phys. **41**, 135213 (2008)
17. G. Gerdin, W. Stygar, F. Venneri, J. Appl. Phys. **52**, 3269 (1981)
18. H. Kelley, A. Marquez, Plasma Phys. Control. Fusion **38**, 1931 (1996)
19. International Centre for Diffraction Data, JCPDS, Card No. PDIS-20iRB (1979)
20. A.S. Albuquerque, J.D. Ardissona, W.A.A. Macedoa, J.L. Lpezb, R. Paniagob, A.I.C. Persianob, J. Magn. Magn. Mater. **226–230**, 1379 (2001)
21. J.F. Zigler, J.P. Biersack, SRIM 2003.20
22. I. Yamada, J. Matsuo, N. Toyoda, Nucl. Instrum. Methods Phys. Res., Sect. B, Beam Interact. Mater. Atoms **206**, 820 (2003)
23. V.N. Popek, S.V. Prasalovich, E.E.B. Campbell, Surf. Sci. **566–568**, 1179 (2004)
24. H.A. Atwer, C.V. Thompson, H.I. Smith, Phys. Rev. Lett. **60**, 112 (1988)
25. D.E. Alexander, G.S. Was, L.E. Rahn, Nucl. Instrum. Methods Phys. Res., Sect. B, Beam Interact. Mater. Atoms **59/60**, 462 (1991)
26. A. Crespo-Sosa, M. Munoz, J.C. Cheang-Wong, A. Oliver, J.M. Saniger, J.G. Banuelos, Appl. Surf. Sci. **206**, 178 (2003)
27. H. Kelly, A. Lepone, A. Marquez, M.J. Sadowski, J. Baranowski, E.S. Sadowska, IEEE Trans. Plasma Sci. **26**, 113 (1998)
28. R. Malik, S. Annapoorni, S. Lamba, P. Sharma, A. Inoue, J. Appl. Phys. **104**, 064317 (2008)
29. M. George, A.M. John, S.S. Nair, P.A. Joy, M.R. Anantharaman, J. Magn. Magn. Mater. **302**, 190 (2006)